Langmuir

Article

pubs.acs.org/Langmuir

Charge-Dependent Transport Switching of Single Molecular Ions in a Weak Polyelectrolyte Multilayer

Lawrence J. Tauzin,[†] Bo Shuang,[†] Lydia Kisley,[†] Andrea P. Mansur,[†] Jixin Chen,[†] Al de Leon,[§] Rigoberto C. Advincula,[§] and Christy F. Landes*[,†,‡]

[†]Department of Chemistry and [‡]Department of Electrical and Chemical Engineering, Rice University, Houston, Texas 77251, United States

[§]Department of Macromolecular Science and Engineering, Case Western Reserve University, Cleveland, Ohio 44106, United States

Supporting Information

ABSTRACT: The tunable nature of weak polyelectrolyte multilayers makes them ideal candidates for drug loading and delivery, water filtration, and separations, yet the lateral transport of charged molecules in these systems remains largely unexplored at the single molecule level. We report the direct measurement of the charge-dependent, pH-tunable, multimodal interaction of single charged molecules with a weak polyelectrolyte multilayer thin film, a 10 bilayer film of poly(acrylic acid) and poly(allylamine hydrochloride) PAA/PAH. Using fluorescence microscopy and single-molecule tracking, two modes of interaction were detected: (1) adsorption, characterized by the molecule remaining immobilized in a subresolution region and (2) diffusion trajectories characteristic of hopping ($D \sim 10^{-9}$ cm^2/s). Radius of gyration evolution analysis and comparison with simulated trajectories confirmed the coexistence of the two transport modes in the same single molecule trajectories. A mechanistic explanation for the probe and condition mediated dynamics is proposed based on a combination of electrostatics and a reversible, pH-induced alteration of the nanoscopic structure of the film. Our results are in good agreement with ensemble studies conducted on similar films, confirm a previously-unobserved hopping mechanism for charged molecules in polyelectrolyte multilayers, and demonstrate that single molecule spectroscopy can offer mechanistic insight into the role of electrostatics and nanoscale tunability of transport in weak polyelectrolyte multilayers.

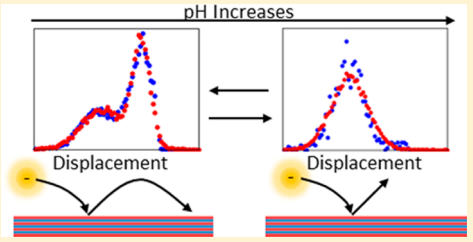

INTRODUCTION

The functionalization of a surface with polyelectrolyte multilayers (PEMs) via layer-by-layer assembly allows the tailoring of surface charge and hydrophobicity.[1,2] Thus, PEM-modified surfaces have been shown to exhibit antifouling properties, and allow for surfaces with variable charge densities.[1,3−5] The assembly of such films is simple, involving only the alternating deposition of polycations and polyanions, yet adjusting several key parameters during assembly allows precise control of the nanoscopic structure of the resulting films. These parameters include the number of layers, the pH and the ionic strength of the deposition solutions, and the selection of the polyelectrolytes themselves.[5−7] For instance, using assembly solutions in which the polyelectrolytes are not fully ionized results in thicker layers and rougher surface topology than those made with fully ionized polyelectrolytes.[8]

When multilayers are constructed using weak polyelectrolytes, their topographical and electronic characteristics can also be tuned post assembly.[9−11] pH affects the dissociation of weak polyelectrolytes, and thus tunes the charge density at the film-solvent interface.[10,12] As a result, the ratio of positive to negative charge near the surface of a PEM film incorporating one or more weak polyelectrolytes can be tuned by adjusting the pH of the solution, and this charge ratio determines not only the electrostatic character of the film, but the nanoscale structure of the film itself.[8,10] In previous research we have shown that changing the degree of ionization of a weak polyelectrolyte brush allows for reversible and charge-selective sequestration of probe molecules,[13] which supports their use in drug release applications.[14,15]

An understanding of the interfacial transport mechanisms that occur within and near these charged and crowded interfaces could help realize the broad application of polyelectrolyte films. Recent work has demonstrated that transport within and near complex environments such as polyelectrolyte films cannot be described by traditional Brownian diffusive models.[16−20] Anomalous diffusion in a polyelectrolyte film can be attributed to confinement of isolated water channels and pockets within the film or hopping from one polyelectrolyte site to another.[21−23] Similar hopping occurs at simple hydrophobic interfaces.[24] The transport of small molecules within the film may also be coupled to the motion of the polyelectrolyte chains themselves.[25,26] Studies that focus specifically on PEM films have found that using a single diffusion coefficient is not adequate to describe the observed transport.[27] Additionally, the rate of diffusion was found to depend on the distance of the probe from the surface of the film.[27] This is attributed to the fact that the outermost layers

Received: March 28, 2014
Revised: May 18, 2014
Published: June 24, 2014

   dx.doi.org/10.1021/la5012007 | Langmuir 2014, 30, 8391−8399

are not as compact as the inner bulk of the film.[27,28] Studies of the dynamics of protein transport on or in a PEM using fluorescence response after photobleaching (FRAP) have shown that the diffusion coefficient and the mobile fraction of the adsorbed protein are dependent on the concentration of the guest molecules and the chemistry of the outermost polyelectrolyte layer.[25,29]

Fluorescence imaging, especially single molecule tracking, enables the direct observation of the dynamics of molecules at interfaces and near or within thin films.[24,30−35] Previous research on transport in polyelectrolytes has indicated that diffusion within polymer films is heterogeneous and that single molecule measurements are required to determine the mechanistic detail of rotational and translational dynamics.[36−43] Reznik et al. found evidence that solute hopping plays a role in the diffusion of charged probes within a poly(styrene sulfonate) brush film using polarization resolved fluorescence correlation spectroscopy (FCS).[37] There are few studies on single molecule dynamic transport in PEMs. An FCS study on diffusion in multilayers composed of poly(styrene sulfonate) and poly(diallyldimethylammonium chloride) found that transport could be described by reversible adsorption/desorption events, as well as confined diffusion.[44] For uncharged probe molecules, two distinct adsorption components were required to adequately model the data, but when a charged probe molecule was used, only one was required; however, charged molecule diffusion was not discussed in detail.[44] Additionally, the autocorrelation analysis used reflects ensemble dynamics determined from a model, not direct observation. The dependence of transport dynamics in PEMs on probe charge and solution pH remains unexplored.

We report on the transport of anionic and cationic probe molecules at a variety of pH values in a PEM, layer-by-layer assembled from the weak polycation poly(allylamine hydrochloride) (PAH) and the weak polyanion poly(acrylic acid) (PAA) measured using single molecule fluorescence microscopy. We performed particle tracking on six different probe/condition pairs: Alexa 555, an anionic probe, as well as Rhodamine 6G (R6G), a cationic probe, at pH 3.5, 5.7, and 8.7. The average number of events per frame was used to demonstrate the pH and charge dependence of probe association with the film. Radius of gyration evolution analysis was used to illustrate the multimodal characteristics of the trajectories. We then extracted quantitative information from the trajectories using the single frame displacement distributions and the diffusion coefficient distributions. Our results demonstrate that molecules undergo reversible adsorption to the PEM, as well as hopping. These findings are consistent with previous bulk studies.[27,45] The degree of association and the presence of confined diffusion is found to depend on the pH of the dye solution and charge of the probe molecules used.

MATERIALS AND METHODS

Substrate Preparation. Prior to multilayer assembly, substrates were cleaned via a multistep process. First, the No. 1 borosilicate glass coverslips (22 × 22 mm, VWR) were sonicated sequentially for 15 min each with water, acetone, and water. The substrates were then treated with piranha solution (70% H_2SO_4 and 30% H_2O_2) for 30 min. The substrates were washed with water to completely remove the piranha solution, dried with compressed air, and then cleaned with oxygen plasma for 3 min. The substrates were immersed in 0.5 vol % aminopropylsilane (APS, Sigma) in dry toluene for 2 h. After washing the substrate with toluene and drying it with compressed air, the functionalized substrate was immersed in 0.1 M HCl for at least an hour.

Multilayer Preparation. One milligram per milliliter of PAA (MW = 1800, Sigma) solution was used as the negatively charged polyelectrolyte solution, while 1 mg/mL of PAH (MW 120,000−200,000, Sigma) was used as the positively charged polyelectrolyte solution. The pH of the PAA and the PAH solutions were adjusted to 3.5 and 7.5 by adding 0.1 M HCl or 0.1 M NaOH, respectively. Sequential dipping was accomplished using an automatic dipper. The APS-functionalized substrate was immersed in PAA solution for 15 min, water for 1 min, PAH solution for 15 min, and water for 1 min. This cycle was repeated until the desired number of bilayers was achieved. For this work, 10 and 20 bilayer films were used. PAH is the outermost layer for all samples. Multilayer thickness was measured using ellipsometry; see the Supporting Information (SI) for details.

Fluorescent Dye Solutions. Solutions of the probe molecules were prepared by diluting Rhodamine 6G (cationic, Sigma) or Alexa Fluor 555 (anionic, Invitrogen) to 10 pM in molecular biology grade water (pH 5.7, Thermo Scientific). HCl (pH 3.5, Sigma-Aldrich) and Tris buffer (pH 8.7, Sigma-Aldrich) were used to adjust aqueous pH.

Fluorescence Measurements. Samples were analyzed using a custom-built total internal reflection wide field fluorescence (TIRF) microscope. A 532 nm diode laser (Coherent, Compass 315M-100SL) was used for excitation. Excitation light was expanded and passed to an oil immersion objective (1.45 NA, 100×, alpha Plan-Fluar, Carl-Zeiss) through a dichroic mirror (Chroma, z532/633rpc). The beam was focused to the edge of the objective such that the angle of incidence on the sample was ∼79° resulting in through-the-objective TIRF. Further details have been published elsewhere.[46] All measurements were conducted with an excitation power density of 1.3 mW/cm^2. Fluorescence emission from the sample was collected through the same objective (epifluorescence) and separated from excitation light by the dichroic mirror, as well as a notch filter (Kaiser, HNPF-532.0-1.0) and a bandpass filter (Chroma, ET585/65m). Emission light was collected using an EMCCD camera (Andor, iXon 897) using an integration time of 30 ms and an EM gain of 300. The recovery time of the camera was 32 ms, resulting in a total time of 62 ms between frames.

A drop of probe solution was added to a multilayer sample and allowed to equilibrate for 20 min to ensure complete hydration of the multilayer prior to measurement. Four thousand frames of data were collected for each sample. Representative frames from each condition can be found in the SI.

Single Molecule Tracking. Data analysis was conducted using custom algorithms written in Matlab R2011b. The raw data from the EMCCD detector was analyzed as a series of two-dimensional images. Details on the molecule identification and tracking method have been published elsewhere.[47−49] Briefly, our program first increases the signal-to-noise ratio (SNR) of each frame by convolution between the frame and a 3 × 3 matrix of ones. This step has been found to be important in tracking algorithms, and increases the SNR by 2 to 3 times.[50] Then, the program calculates the local background and local noise level. The corresponding local intensity threshold was set to the local background plus three times the standard deviation of local noise. Particles were preidentified as pixels having local

dx.doi.org/10.1021/la5012007 | Langmuir 2014, 30, 8391−8399

maximum intensities greater than this threshold. The local maximum intensity is compared to other pixels within an input distance. We used a 3 pixel distance for all our analyses. Next, the centers of all the preidentified particles were calculated using a radial symmetry algorithm.[51] The second moment of the particle is compared with the second moment of the same fitting region with Gaussian noise. Only if the second moment of the particle is smaller than 90% of the second moment of the Gaussian noise will we consider the particle a real particle and record its position. Finally, we used a nearest neighbor algorithm to generate molecular trajectories.[47,52] See the SI for a sample of raw data (File la5012007_si_001.avi) and the same data overlaid with tracking results (File la5012007_si_002.avi).

RESULTS AND DISCUSSION

We measured trajectories of cationic R6G and anionic Alexa 555 diffusing on the surface of a 10 bilayer PAA/PAH multilayer in molecular biology grade water (pH 5.7), HCl (pH 3.5), and Tris buffer (pH 8.7). We begin with a discussion of the ionization state of the probes and film at the different pH conditions as this is crucial to the interpretation of the results. The degree of interaction of the probe molecules is used to show the pH-dependence of the interaction of the probe molecules with the multilayer. Radius of gyration evolution analysis is used to determine that under certain probe-condition combinations transport is characterized by intermittent surface adsorption. Analysis of the single frame displacement and diffusion coefficient histograms is used to further characterize the tunability of film interaction for the various probe-condition pairs. Finally, these results are used to develop an interaction mechanism based on electrostatic interactions of the probes with the outermost layer of the film.

Film/Probe Ionization. The charge density at the interface changes with the pH value of the solution during film assembly and during the measurements. Work by Rubner and others has demonstrated that the pK_a of a polyelectrolyte can be shifted by up to four pH units when the polyelectrolytes are incorporated into a multilayer compared to the pK_a in solution.[10,53] According to their measurements, in our HCl solutions (pH 3.5) PAA should be approximately 87% ionized while PAH should be close to 100% ionized. In MB water (pH 5.7) PAA becomes slightly more ionized ~90% while PAH remains nearly completely ionized. In Tris buffer (pH 8.7) PAA becomes still more ionized reaching >90% ionization while PAH becomes slightly less ionized ~90%. It should be noted that the actual degree of ionization values post assembly are difficult to quantify as they not only depend on the chosen polyelectrolyte pair, but the assembly pH of the polymer solutions.[10] The inner layers of the film are uncharged due to the intrinsic charge compensation that holds the multilayer together.[6] Because the PAH is part of a multilayer, most of the charge in the outermost layer will be compensated by the underlying PAA layer, but we expect some positive charge to remain to facilitate the charge overcompensation mechanism that is essential for multilayer assembly.[54]

The probes are also ionized in the solution differently at different pH values. Alexa 555 is a strong acid based on its sulfonate functional groups and as such, all of the molecules are negatively charged under all three conditions. The pK_a of R6G is 7.5,[55] so the molecules are fully ionized (positively charged) at pH = 3.5, 60% ionized at pH = 5.7 and 6% ionized at pH = 8.7.

The molecular structure of the probe molecules (Alexa 568 instead of Alexa 555 because the structure of Alexa 555 is proprietary) as well as those of PAA and PAH are shown in Figure 1 (a, b, c, and d). Because of the excitation geometry and

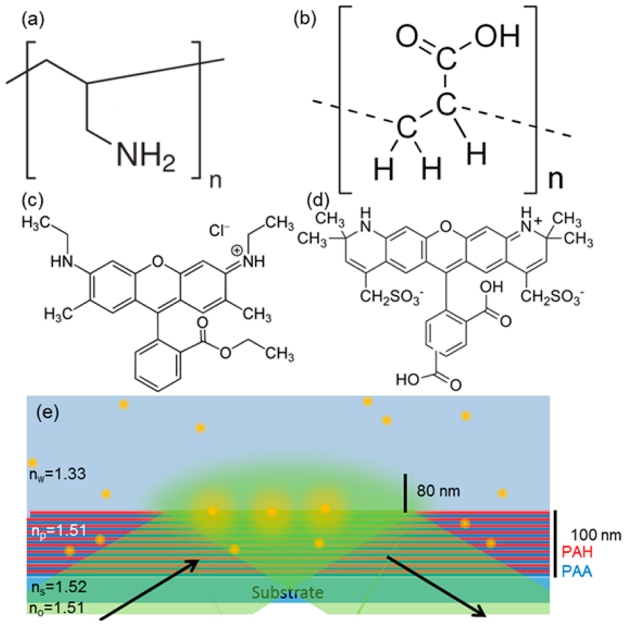

Figure 1. Experimental setup and details. (a) Molecular structures of PAH, (b) PAA, (c) R6G, and (d) Alexa 568. (e) Schematic showing the excitation of probe molecules via TIRF. The refractive indices of water, polymer film, glass substrate, and objective oil are also shown.

integration time of 30 ms, probes diffusing freely in solution ($D \approx 10^8$ nm^2/s)[38] are visible only as a constant background signal and are therefore not counted during particle identification.[48] Probes adsorbed in the film bulk will bleach a short time after the sample is illuminated. Most of the events, therefore, are new molecules associated with the film surface that subsequently either diffuse back into solution or remain within the film until they photobleach. In order to verify that the algorithm is correctly linking trajectories, the order of the frames from 1000 frames worth of experimental data was randomly shuffled,[24] and the data was reanalyzed, producing only 44 trajectories greater than the 5 frame cutoff used for analysis, compared to 1248 trajectories for the unshuffled data. This result suggests that erroneous linking of different molecules is rare (< 4% false positives).

Based on previous studies[6,44] and our experimental design, the molecules we observe are expected to be probe molecules interacting with the outermost layers of the polymer film as depicted in the experimental cartoon in Figure 1e. Intensity measurements confirm that the TIRF condition occurs at the film water interface as depicted in Figure 1e. See the SI for details. While we cannot rule out observation of diffusion within the film bulk, adsorption of probe molecules in a PEM has been shown to be dependent on salt concentration.[44] Schlenoff et al. have reported that residual salt is only found in the outermost layer of the PEM, which strongly suggests that we are observing probe interaction near the outer interface of the PEM.[6]

Probe Association. The strongest probe−surface interaction exists for Alexa 555 in HCl and R6G in Tris buffer (Figure 2a and 2g). The number of events per frame was

dx.doi.org/10.1021/la5012007 | Langmuir 2014, 30, 8391−8399

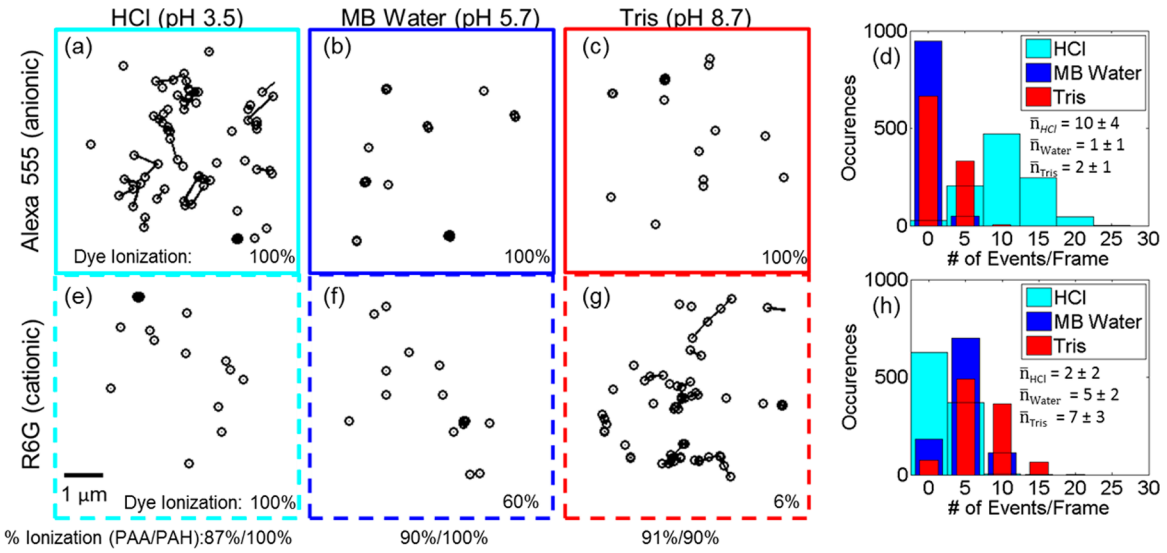

Figure 2. (a,b,c) 50 frames of trajectories measured in the same area for Alexa 555 over the 10 bilayer film in HCl, MB water, and Tris buffer, respectively. (e,f,g) 50 frames of trajectories measured in the same area for R6G over the 10 bilayer film in HCl, MB water, and Tris buffer, respectively. The predicted ionization state of the probes and multilayer are also shown. (d,h) Histograms showing the number of particles identified per frame for Alexa 555 and R6G respectively for the various conditions along with the average number of events per frame for each probe-condition combination (averaged over 1000 frames). Bar width is cosmetic. Border color and style correspond to the probes: Alexa 555 (solid) and R6G (dashed) and conditions: pH 3.5 (cyan), pH 5.7 (blue), and pH 8.7 (red).

calculated by averaging the number of new objects appearing per frame. For Alexa 555, there is a decrease in probe association when pH is increased, from an average of 10 ± 4 events per frame in HCl, to 1 ± 1 in MB water, and 2 ± 1 in Tris buffer (Figure 2d). Generally, the opposite is true for R6G (Figure 2h). As the pH is decreased, there is somewhat less association of R6G with the film, from an average number of events per frame of 7 ± 3 in Tris to 5 ± 2 in MB water to 2 ± 2 in HCl, although the distributions overlap considerably (Figure 2d).

Two distinct types of trajectory profiles, seen in Figure 2, indicate the presence of at least two modes of interaction between the probes and film, depending on the solution pH and probe charge. For the conditions with the fewest number of events per frame (Alexa in MB water and Tris buffer Figure 2b,c, and R6G in MB water and HCl Figure 2e,f), trajectories are mostly adsorption events. We either observe a molecule for 1 frame or less, or we observe the same molecule over multiple frames at the same location within our static localization error (~40 nm). However, for Alexa in HCl and R6G in Tris, there is an additional type of trajectory involving adsorption of the molecule followed by the movement of the molecule to an adjacent location. These trajectories are indicative of hindered diffusion that is slow enough for us to track with our integration time. As we will demonstrate with radius of gyration evolution analysis and an examination of the single frame displacement distributions, we are observing molecules undergoing intermittent surface diffusion, or "hopping" from one location on the surface to another, similar to the desorption mediated diffusion identified by the Schwartz group for molecules diffusing at a solid-liquid interface,[24] and the hopping we previously identified in polyelectrolyte brushes.[37] We do not find repeat adsorption events at specific sites that would be characteristic of "hot spots", which have been observed in inorganic substrates such as silica due to defects.[56] Because hopping behaviors are important for molecular transport near and within the film, we will focus our efforts on the conditions where trajectories show hopping behavior (examples shown in Figure 2a,g).

Radius of Gyration Evolution Analysis. Radius of gyration evolution[17,57] quantitatively distinguishes periods of immobilization vs diffusion within a trajectory, and was used to further analyze the diffusive trajectories. This technique has been used previously to study systems displaying intermittent surface interaction.[17,57] The radius of gyration of a particle (R_g) is calculated at each point in the trajectory using the following equation:[17,57]

$$R_g = \sqrt{R_1^2 + R_2^2} \tag{2}$$

where R_1 and R_2 correspond to the major and minor eigenvalues of the radius of gyration tensor T. The tensor corresponds to the 2 by 2 matrix:

$$T = \begin{pmatrix} \frac{1}{N}\sum_{i=1}^{N}(x_i - \langle x\rangle)^2 & \frac{1}{N}\sum_{i=1}^{N}(x_i - \langle x\rangle)(y_i - \langle y\rangle) \\ \frac{1}{N}\sum_{i=1}^{N}(x_i - \langle x\rangle)(y_i - \langle y\rangle) & \frac{1}{N}\sum_{i=1}^{N}(y_i - \langle y\rangle)^2 \end{pmatrix} \tag{3}$$

where N is the number of steps in the trajectory, x and y are the x and y locations of the particle. The evolution of the radius of gyration with time is established by calculating R_g for each time step in a trajectory.

The radius of gyration evolution was evaluated using simulated trajectories. Figure 3a shows the radius of gyration evolution of simulated Brownian trajectories generated with a 2D off lattice Monte Carlo random walk model and simulated trajectories with periods of adsorption. Displacements were drawn from normal distributions with widths corresponding to D = 0.01 $\mu m^2/s$ for the Brownian trajectories, and $D_{unconfined}$ = 0.1 $\mu m^2/s$ and $D_{confined}$ = 0.0001 $\mu m^2/s$ for the trajectories with periods of confinement. Diffusors had a 40% chance of becoming immobilized and once immobilized had a 10% chance of becoming mobile again. (See SI for further details).

dx.doi.org/10.1021/la5012007 | Langmuir 2014, 30, 8391−8399

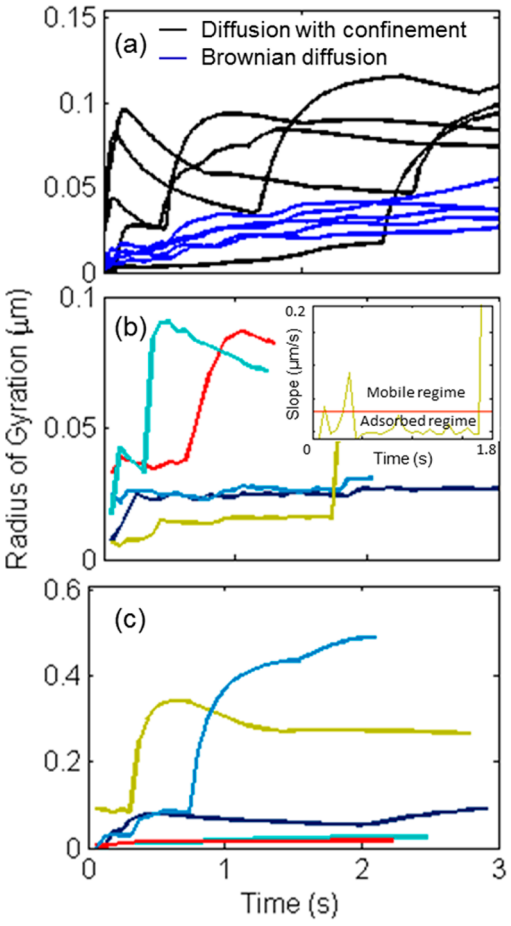

Figure 3. Radius of gyration evolution analysis. (a) Shows radius of gyration evolution curves for simulated Brownian motion with D = 0.01 $\mu m^2/s$ (blue) and diffusion with confinement with D = 0.1 $\mu m^2/s$ and D_{conf} = 0.0001 $\mu m^2/s$ (black). (b) Five trajectories of Alexa 555 in acid over a 10 bilayer PAA/PAH film. The inset is a plot of the instantaneous slope of the yellow-green curve in panel b with a red line drawn at the threshold used to determine whether or not the molecule was stationary at each step. (c) Five trajectories of R6G in Tris buffer over a 10 bilayer PAA/PAH film.

The radius of gyration evolution plots of the Brownian trajectories differ substantially from those of trajectories with periods of adsorption. For Brownian trajectories, the radius of gyration increases at a reasonably constant rate. Conversely, the slope of the radius of gyration evolution for trajectories with adsorption is not constant. When the slope is near 0, the particle is adsorbed. When the probe jumps to a new location, there is a large increase in slope. Small negative slopes in the radius of gyration are observed after large displacements because the radius of gyration is effectively a running average with a $1/N$ dependency.

Evaluation of radius of gyration evolution for experimental trajectories demonstrates that the same molecule can switch between periods of adsorption and hopping. Radius of gyration versus time plots for five trajectories each of Alexa 555 in HCl (pH = 3.5) and R6G in Tris buffer (pH = 8.7) are shown in Figure 3b,c. Like the radius of gyration evolution plots for the simulated trajectories with adsorption, these trajectories show distinct regions of adsorption and hopping to a new area. In order to estimate how often particles are adsorbed, a threshold is set equal to 0 plus 1.5 times the standard deviation of the instantaneous slope of all trajectories. We categorize instantaneous slope values below this threshold as adsorbed. The instantaneous slope of the yellow-green line in Figure 3b and the threshold are plotted in the inset of Figure 3. Using this rough estimation, we find that on average, Alexa 555 molecules in HCl spend more than 82% of their tracking time adsorbed, while R6G molecules in Tris buffer spend more than 91% of their tracking time adsorbed. While the radius of gyration analysis works well for our short trajectories, it should be noted that such analysis is not appropriate for longer trajectories as switching behavior becomes more difficult to detect near the end of long trajectories. Methods such as sliding time window mean squared displacement methods would be more appropriate for long trajectories.[57]

Single Frame Displacement. Analysis of the single frame displacements is an effective method to quantify different mechanistic dynamics.[56] The single frame displacement is simply the distance that a tracked molecule moves from one frame to the next. This analysis can also provide the average diffusion constants of the different transport modes. We analyze the single frame displacement data by generating histograms using all displacement events in a given sample. The mean and relative population of the distributions is determined by using a Markov Chain Monte Carlo (MCMC) algorithm to generate model distributions that are as close as possible to the experimental data (see the SI for the algorithm used). The MCMC algorithm can be compared to fitting the histograms; however, it equally evaluates every data point and is independent of the bin size. An analysis of the single frame displacements of the two probe molecules Alexa 555 and R6G under the three different pH conditions confirms the presence of two modes. Figure 4 shows histograms of the single frame displacement (black dots) along with a model distribution calculated using the MCMC algorithm (gray dots). The distribution of the displacements in log scale demonstrates that there are two populations: one representing adsorbed particles characterized by short displacement steps indistinguishable from the localization uncertainty, and one representing long displacement steps attributed to hopping or confined diffusion.

The short displacements are on average ~40 nm, and represent immobile molecules. We do not expect adsorbed probe molecules to appear completely stationary due to the localization uncertainty of our radial symmetry fitting algorithm, which can vary due to experimental parameters such as microscope focus. There are also long displacements of more than an order of magnitude greater than the adsorbed displacements which are characteristic of mobile or hopping molecules. Three of the six probe-pH combinations exhibit these hopping displacements: Alexa in HCl (Figure 4a), R6G in Tris (Figure 4f), and a small population of R6G in HCl (Figure 4b). There is also a small population of hopping molecules for R6G in water (Figure 4d), but the contribution to the overall distribution is so small that the center of the second distribution cannot be calculated properly. The good agreement between the experimental data and the simulated MCMC data confirms that our analytical results are consistent with two coexisting modes of transport at the film water interface.

The relative populations of the immobilized and hopping distributions indicate that R6G is immobilized 20% more frequently than Alexa. For Alexa in HCl the probability of an event belonging to the adsorbed distribution is 55%, while the probability that it belongs to the hopping distribution is 45%. For R6G in HCl, the probabilities are 69% and 31% for the

dx.doi.org/10.1021/la5012007 | Langmuir 2014, 30, 8391−8399

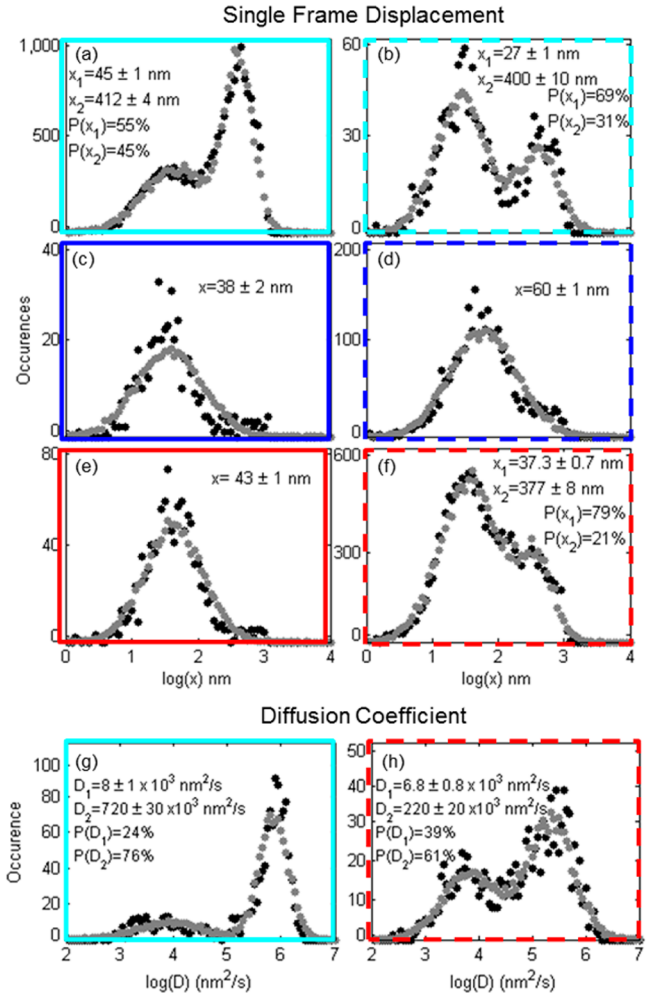

Figure 4. Single frame displacement histograms and diffusion coefficient histograms for each probe at the three different pH conditions. (a,c,e) Single frame displacement histograms (black) and MCMC approximation of the distribution (gray) for Alexa 555 in HCl, MB water, and Tris buffer, respectively. (b,d,f) Single frame displacement histograms (black) and MCMC approximation of the distribution (gray) for R6G in HCl, MB water, and Tris buffer, respectively. Parameters extracted from the distribution, assuming log-normal distributions, are also indicated, including the mean displacement for each distribution as well as the probability of a displacement belonging to a distribution (if applicable). (g,h) Distributions of the diffusion coefficient calculated from each individual trajectory (black) and MCMC approximation of the distribution using the shown parameters (gray) for Alexa 555 in HCl and R6G in Tris buffer, respectively. Parameters shown are the average D for each distribution and the probability of a trajectory having a D that falls into that distribution. Border color and style correspond to the probes: Alexa 555 (solid), and R6G (dashed) and conditions: pH 3.5 (cyan), pH 5.7 (blue), and pH 8.7 (red).

adsorbed and hopping distributions respectively, and for R6G in Tris those probabilities are 79% and 21%. Clearly, based on these distributions, R6G is less likely to hop from one site to another regardless of the pH of the solution. We expect uncompensated PAH in the outermost layer of the film to provide adsorption sites for oppositely charged Alexa 555 molecules. If these sites are close together, then the Alexa molecules can easily hop between them. Uncompensated PAA would provide appropriate adsorption sites for R6G, but PAA is not the outermost layer of the multilayer; therefore, we expect R6G to have limited access to these sites, which may explain why we see a lower probability of hopping for R6G.

The distributions of the diffusion coefficients (Figure 4g,h) also show two clear populations, further evidence of two dynamic processes. The diffusion coefficient summarizes the average displacement of each single molecule over its observation period, and is calculated by averaging the squared displacements of each step in the trajectory.[58] The slower diffusion distribution is centered at $\sim 7 \times 10^3$ nm^2/s for both the Alexa and R6G probes, and corresponds to molecules that are adsorbed in the film. The value arises primarily due to errors in location identification. The faster diffusion coefficient is $720 \pm 30 \times 10^3$ nm^2/s for Alexa 555 in HCl, while for R6G in Tris, it is somewhat slower, $220 \pm 20 \times 10^3$ nm^2/s. These diffusion coefficients are 1−2 orders of magnitude slower than previous measurements of small molecules diffusing in PEM films, where the lateral diffusion coefficients of single neutral probes are on the order of 10^8 nm^2/s.[44] The slower diffusion that we measured could be due to the fact that our probes are charged, unlike the neutral probes used in the previous study,[44] the result of a different polymer system, or molecules that remain immobilized for the entire observation period. See the SI for discussion of a neutral probe.

In both cases, a molecule is more likely to have a diffusion coefficient that belongs to the faster diffusion distribution: 76% for Alexa in HCl, and 61% for R6G in Tris. While this may seem to contradict our previous conclusions that molecules are most likely to get stuck, it is not surprising because the diffusion coefficient is determined from the mean squared displacement of a trajectory that is calculated from all of the single frame displacement events for each particular molecule. Scatter plots of D vs trajectory length (Figure S5) show that some of the shortest trajectories (less than 10 frames) produce the fastest diffusion coefficients. These are likely trajectories in which the molecules are hopping for the duration of the trajectory and escape the TIRF excitation volume before they become immobilized in the film. Thus, at least two types of trajectories contribute to the distributions of D: short trajectories where the molecules are continuously hopping, and longer trajectories that contain periods of immobilization.

Photophysics due to blinking or bleaching is not a major contributor to our ability to characterize the relative difference between adsorbed and hopping displacements. The experiments were repeated with the laser power set to 5, 10, and 15 mW (corresponding to 1.67, 3.33, and 5 mW/cm^2) in order to ensure that our measurements were not significantly perturbed by photophysics. In the case of both Alexa in HCl and R6G in Tris, the average single frame displacement for the adsorbed and hopping distribution does not change as the power increases (data not shown), and the percent of single frame displacements belonging to the adsorbed distribution decreased by ∼5% after the power was increased by 200% (Figure 5). Despite this small increase, the overall difference in the relative population of the adsorbed distributions of Alexa 555 and R6G remains 22%, suggesting that the higher probability of R6G to become adsorbed is not an artifact of photophysics.

Proposed Mechanism of the Probe-Film Interactions. The explanation for the probe and condition mediated dynamics is likely a combination of hydrophobic interactions along with electrostatics and a change in film density, which are reversibly tuned by the pH of the solution. Such a shift in pH causes changes to the relative degree of polyelectrolyte ionization as discussed previously. Farhat et al. found that the

dx.doi.org/10.1021/la5012007 | Langmuir 2014, 30, 8391−8399

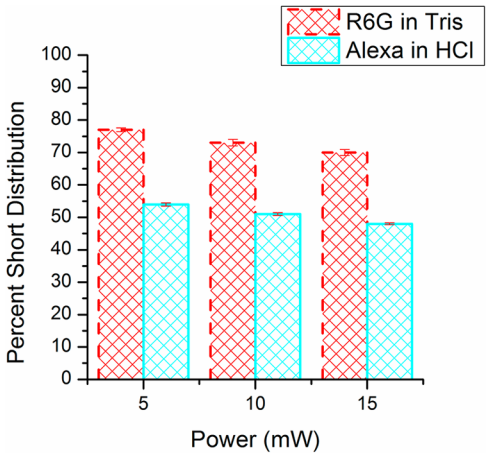

Figure 5. Percent single frame displacements belonging to the adsorbed distribution as a function of laser power for R6G in Tris buffer and Alexa 555 in HCl. The error bars are based on the standard deviation of the sampling values of p (the probability of adsorption) that we have defined in the SI.

transport of ions through a PEM was an electrostatic process governed by hopping of the ions from one charged site in the PEM to another.[21] We used this work as the basis to develop an electrostatic based mechanism for the tunable surface interactions we measure. Because hydrophobic interactions are also important for interfacial transport, we probed the contribution of hydrophobic interactions by measuring the diffusion of Rhodamine B, a molecule with no net charge in water, over the PEM. We find that the degree of association characterized by the number of events per frame is similar to that of the charged probes in water, but the single frame displacement distribution is drastically different with two clear distributions instead of one, strongly supporting the notion that electrostatic interactions are the primary determinant for how molecules interact with the film. See the SI for details.

For R6G in HCl, both the ionization of the probe and outer film layer promote repulsion of the probe molecules. As the pH is increased, the probe molecules become less ionized, as does the film to a much lesser degree, allowing for the increased interaction of R6G with the film that we measure. For Alexa 555 in HCl, the near complete ionization of the probe and film create an electrostatic environment that supports interaction, which is what we observe. This electrostatic attraction also explains the hopping behavior, as probe molecules are more likely to interact with the film repeatedly after diffusing away. However, as the pH is increased, there is drastically decreased interaction of the probe with the film, even though we expect both to remain mostly ionized. This observation is not intuitive and difficult to explain, but could be due to a complex interplay of electrostatic effects combined with steric and hydrophobic effects. For instance, Yip and Lee found that Coulombic repulsion had a negligible effect on the loading of cationic R6G molecules in a cationic polymer film, while significant loading enhancement was found when using a negatively charged dye in the same film. They conclude that Coulombic attraction can play a significantly larger role on the incorporation of molecules into a PEM than Coulombic repulsion,[59] illustrating that the electrostatic interactions of molecules in PEMs are complicated and still not well understood.

It is possible that structural properties of the film, such as film density, reflecting the spatial configuration of the polymer chains, contribute to the degree of association of the probes with the film. According to the estimates for the degree of ionization discussed above, there should be a change in film structure upon the change in pH from 3.5 to 8.7. At a pH of 3.5 there is a difference in the degree of ionization of PAH (nearly fully ionized) and PAA (87% ionized). This suggests that the structure of the film under these conditions will be less compact than at higher pH values due to less intrinsic charge compensation. Such a film is expected be thick, with loops forming in the polymer chains resulting in a film that is less compact.[8,10,60] This could explain why both probes appear to interact with the film under acidic conditions, although R6G interaction is not very favorable, suggesting that the dynamics are not purely sterically mediated. It has been found that films constructed of polyelectrolytes that are nearly fully ionized are thinner and contain more ordered polymer networks.[10] It is therefore reasonable to assume that contraction of the film will occur as pH is decreased, resulting in a comparatively more dense film, which could explain the apparent exclusion of both probes in water. Upon increasing the pH to 8.7, the PAH becomes less ionized, which could result in a swelling of the film similar to that in a solution of pH 3.5. This swelling combined with a decrease in ionization of the cationic PAH and increase in ionization of the anionic PAA may create an environment less hostile to R6G-film interaction.

CONCLUSIONS

We demonstrate pH-dependent hopping of charged probe molecules within a PAA/PAH PEM in addition to reversible adsorption of probe molecules. These two transport modes exist for Alexa 555 at pH 3.5 and R6G at pH 8.7 but not for Alexa at pH 8.7 or R6G at pH 3.5 or either probe in MB water (pH 5.7), with only adsorption present for the other probe-condition pairs studied, resulting in tunable behavior based on probe charge and solution pH. Radius of gyration evolution analysis shows that for Alexa in HCl and R6G in Tris, the transport at the surface is governed by intermittent adsorption events. Cationic R6G is less likely to hop from one location to another under all conditions compared to anionic Alexa 555, and we confirm that the tendency of R6G to remain adsorbed is not related to photophysics. We propose an electrostatic-based interaction mechanism to explain our results. At low pH, excess positive charge in the outer layers of the film promotes interaction with the anionic probe, while the cationic probe is largely excluded. At high pH, the cationic sites in the outer layer are sparser, resulting in decreased interaction of the anionic probes. The reversible transport tuning we demonstrate moves us one step closer to the creation of optimal functionalized surfaces for specialized applications in water filtration and remediation, drug loading and release, and ion exchange separations.

ASSOCIATED CONTENT

Supporting Information

Ellipsometry characterization of LbL films, AFM characterization of the LbL films, a discussion on the location of the evanescent wave, raw data, explanation of MCMC algorithm, and simulation details, scatter plots of D vs trajectory length, and Rhodamine B data. Videos showing raw fluorescence data of R6G in Tris over the 10 bilayer film (File la5012007_si_001.avi) and the same data overlaid with particle identification and trajectories Frame rate decreased by 50%

dx.doi.org/10.1021/la5012007 | Langmuir 2014, 30, 8391−8399

for clarity (File la5012007_si_002.avi). This material is available free of charge via the Internet at http://pubs.acs.org/.

AUTHOR INFORMATION

Corresponding Author

*E-mail: cflandes@rice.edu.

Notes

The authors declare no competing financial interest.

ACKNOWLEDGMENTS

C.F.L. acknowledges the Welch Foundation (Grant C-1787), the National Science Foundation (NSF; Grants CBET-1134417 and CHE-1151647), and the National Institutes of Health (NIH; Grant GM94246-01A1). L.K. acknowledges the NSF Graduate Research Fellowship (Grant 0940902). The Advincula group acknowledges the National Science Foundation (NSF 1333651). The authors also thank Stephan Link and his group for helpful suggestions.

REFERENCES

(1) Tang, Z. Y.; Wang, Y.; Podsiadlo, P.; Kotov, N. A. Biomedical Applications of Layer-by-Layer Assembly: From Biomimetics to Tissue Engineering. *Adv. Mater.* **2006**, *18*, 3203−3224.

(2) Zhai, L.; Cebeci, F. C.; Cohen, R. E.; Rubner, M. F. Stable Superhydrophobic Coatings from Polyelectrolyte Multilayers. *Nano Lett.* **2004**, *4*, 1349−1353.

(3) Lichter, J. A.; Van Vliet, K. J.; Rubner, M. F. Design of Antibacterial Surfaces and Interfaces: Polyelectrolyte Multilayers as a Multifunctional Platform. *Macromolecules* **2009**, *42*, 8573−8586.

(4) Caruso, F.; Lichtenfeld, H.; Donath, E.; Mohwald, H. Investigation of Electrostatic Interactions in Polyelectrolyte Multilayer Films: Binding of Anionic Fluorescent Probes to Layers Assembled onto Colloids. *Macromolecules* **1999**, *32*, 2317−2328.

(5) Lowack, K.; Helm, C. A. Molecular Mechanisms Controlling the Self-Assembly Process of Polyelectrolyte Multilayers. *Macromolecules* **1998**, *31*, 823−833.

(6) Schlenoff, J. B.; Dubas, S. T. Mechanism of Polyelectrolyte Multilayer Growth: Charge Overcompensation and Distribution. *Macromolecules* **2001**, *34*, 592−598.

(7) Sui, Z.; Salloum, D.; Schlenoff, J. B. Effect of Molecular Weight on the Construction of Polyelectrolyte Multilayers: Stripping versus Sticking. *Langmuir* **2003**, *19*, 2491−2495.

(8) Shiratori, S. S.; Rubner, M. F. pH-Dependent Thickness Behavior of Sequentially Adsorbed Layers of Weak Polyelectrolytes. *Macromolecules* **2000**, *33*, 4213−4219.

(9) Stuart, M. A. C.; Huck, W. T. S.; Genzer, J.; Muller, M.; Ober, C.; Stamm, M.; Sukhorukov, G. B.; Szleifer, I.; Tsukruk, V. V.; Urban, M.; et al. Emerging Applications of Stimuli-Responsive Polymer Materials. *Nat. Mater.* **2010**, *9*, 101−113.

(10) Choi, J.; Rubner, M. F. Influence of the Degree of Ionization on Weak Polyelectrolyte Multilayer Assembly. *Macromolecules* **2004**, *38*, 116−124.

(11) Hou, Y.; Liu, G.; Wu, Y.; Zhang, G. Reentrant Behavior of Grafted Poly(sodium styrenesulfonate) Chains Investigated with a Quartz Crystal Microbalance. *Phys. Chem. Chem. Phys.* **2011**, *13*, 2880−2886.

(12) Longo, G. S.; Cruz, M. O. d. l.; Szleifer, I. Molecular Theory of Weak Polyelectrolyte Thin Films. *Soft Matter* **2012**, *8*, 1344−1354.

(13) Daniels, C. R.; Tauzin, L. J.; Foster, E.; Advincula, R. C.; Landes, C. F. On the pH-Responsive, Charge-Selective, Polymer-Brush-Mediated Transport Probed by Traditional and Scanning Fluorescence Correlation Spectroscopy. *J. Phys. Chem. B* **2013**, *117*, 4284−4290.

(14) Luo, Y.; Yao, X.; Yuan, J.; Ding, T.; Gao, Q. Preparation and Drug Controlled-Release of Polyion Complex Micelles as Drug Delivery Systems. *Colloids Surf., B* **2009**, *68*, 218−224.

(15) Wang, X.; Yang, Y.; Liao, Y.; Yang, Z.; Jiang, M.; Xie, X. Robust Polyazobenzene Microcapsules with Photoresponsive Pore Channels and Tunable Release Profiles. *Eur. Polym. J.* **2012**, *48*, 41−48.

(16) Wang, B.; Anthony, S. M.; Bae, S. C.; Granick, S. Anomalous yet Brownian. *Proc. Natl. Acad. Sci. U. S. A.* **2009**, DOI: 10.1073/pnas.0903554106.

(17) Elliott, L. C. C.; Barhoum, M.; Harris, J. M.; Bohn, P. W. Single Molecule Tracking Studies of Lower Critical Solution Temperature Transition Behavior in Poly(*N*-isopropylacrylamide). *Langmuir* **2011**, *27*, 11037−11043.

(18) Raccis, R.; Roskamp, R.; Hopp, I.; Menges, B.; Koynov, K.; Jonas, U.; Knoll, W.; Butt, H. J.; Fytas, G. Probing Mobility and Structural Inhomogeneities in Grafted Hydrogel Films by Fluorescence Correlation Spectroscopy. *Soft Matter* **2011**, *7*, 7042−7053.

(19) Cherdhirankorn, T.; Retsch, M.; Jonas, U.; Butt, H.-J.; Koynov, K. Tracer Diffusion in Silica Inverse Opals. *Langmuir* **2010**, *26*, 10141−10146.

(20) Rodríguez Presa, M. J.; Gassa, L. M.; Azzaroni, O.; Gervasi, C. A. Estimating Diffusion Coefficients of Probe Molecules into Polyelectrolyte Brushes by Electrochemical Impedance Spectroscopy. *Anal. Chem.* **2009**, *81*, 7936−7943.

(21) Farhat, T. R.; Schlenoff, J. B. Doping-Controlled Ion Diffusion in Polyelectrolyte Multilayers: Mass Transport in Reluctant Exchangers. *J. Am. Chem. Soc.* **2003**, *125*, 4627−4636.

(22) Jagannathan, K.; Sung, B. J.; Yethiraj, A. Dynamics of Probes in Model Glassy Matrices. *Phys. Rev. Lett.* **2006**, *97*, 145503.

(23) Wang, S.; Jing, B.; Zhu, Y. Single Molecule Diffusion on Hard, Soft and Fluid Surfaces. *RSC Adv.* **2012**, *2*, 3835−3843.

(24) Skaug, M. J.; Mabry, J.; Schwartz, D. K. Intermittent Molecular Hopping at the Solid−Liquid Interface. *Phys. Rev. Lett.* **2013**, *110*, 256101.

(25) Vogt, C.; Ball, V.; Mutterer, J.; Schaaf, P.; Voegel, J. C.; Senger, B.; Lavalle, P. Mobility of Proteins in Highly Hydrated Polyelectrolyte Multilayer Films. *J. Phys. Chem. B* **2012**, *116*, 5269−5278.

(26) Wang, S.; Zhu, Y. Molecular Diffusion on Surface Tethered Polymer Layers: Coupling of Molecular Thermal Fluctuation and Polymer Chain Dynamics. *Soft Matter* **2010**, *6*, 4661−4665.

(27) Klitzing, R. v.; Möhwald, H. A Realistic Diffusion Model for Ultrathin Polyelectrolyte Films. *Macromolecules* **1996**, *29*, 6901−6906.

(28) Ladam, G.; Schaad, P.; Voegel, J. C.; Schaaf, P.; Decher, G.; Cuisinier, F. In Situ Determination of the Structural Properties of Initially Deposited Polyelectrolyte Multilayers. *Langmuir* **2000**, *16*, 1249−1255.

(29) Szyk, L.; Schwinté, P.; Voegel, J. C.; Schaaf, P.; Tinland, B. Dynamical Behavior of Human Serum Albumin Adsorbed on or Embedded in Polyelectrolyte Multilayers. *J. Phys. Chem. B* **2002**, *106*, 6049−6055.

(30) Flier, B. M. I.; Baier, M.; Huber, J.; Mullen, K.; Mecking, S.; Zumbusch, A.; Woll, D. Single Molecule Fluorescence Microscopy Investigations on Heterogeneity of Translational Diffusion in Thin Polymer Films. *Phys. Chem. Chem. Phys.* **2011**, *13*, 1770−1775.

(31) Bhattacharya, S.; Sharma, D. K.; Saurabh, S.; De, S.; Sain, A.; Nandi, A.; Chowdhury, A. Plasticization of Poly(vinylpyrrolidone) Thin Films under Ambient Humidity: Insight from Single-Molecule Tracer Diffusion Dynamics. *J. Phys. Chem. B* **2013**, *117*, 7771−7782.

(32) Koynov, K.; Butt, H.-J. Fluorescence Correlation Spectroscopy in Colloid and Interface Science. *Curr. Opin. Colloid Interface Sci.* **2012**, *17*, 377−387.

(33) Woll, D. Fluorescence Correlation Spectroscopy in Polymer Science. *RSC Adv.* **2014**, *4*, 2447−2465.

(34) Hutchison, J. A.; Uji-i, H.; Deres, A.; Vosch, T.; Rocha, S.; Muller, S.; Bastian, A. A.; Enderlein, J.; Nourouzi, H.; Li, C.; et al. A Surface-Bound Molecule that Undergoes Optically Biased Brownian Rotation. *Nat. Nanotechnol.* **2014**, *9*, 131−136.

(35) Kastantin, M.; Walder, R.; Schwartz, D. K. Identifying Mechanisms of Interfacial Dynamics Using Single-Molecule Tracking. *Langmuir* **2012**, *28*, 12443−12456.

(36) Daniels, C. R.; Reznik, C.; Kilmer, R.; Felipe, M. J.; Tria, M. C. R.; Kourentzi, K.; Chen, W. H.; Advincula, R. C.; Willson, R. C.;

Landes, C. F. Permeability of Anti-Fouling PEGylated Surfaces Probed by Fluorescence Correlation Spectroscopy. *Colloids Surf., B* **2011**, *88*, 31−38.
(37) Reznik, C.; Berg, R.; Foster, E.; Advincula, R.; Landes, C. F. Transient Three-Dimensional Orientation of Molecular Ions in an Ordered Polyelectrolyte Membrane. *J. Phys. Chem. Lett.* **2011**, *2*, 592−598.
(38) Reznik, C.; Darugar, Q.; Wheat, A.; Fulghum, T.; Advincula, R. C.; Landes, C. F. Single Ion Diffusive Transport within a Poly(styrene sulfonate) Polymer Brush Matrix Probed by Fluorescence Correlation Spectroscopy. *J. Phys. Chem. B* **2008**, *112*, 10890−10897.
(39) Reznik, C.; Estillore, N.; Advincula, R. C.; Landes, C. F. Single Molecule Spectroscopy Reveals Heterogeneous Transport Mechanisms for Molecular Ions in a Polyelectrolyte Polymer Brush. *J. Phys. Chem. B* **2009**, *113*, 14611−14618.
(40) Fowlkes, J. D.; Collier, C. P. Single-Molecule Mobility in Confined and Crowded Femtolitre Chambers. *Lab Chip* **2013**, *13*, 877−885.
(41) Karatasos, K.; Krystallis, M. Dynamics of Counterions in Dendrimer Polyelectrolyte Solutions. *J. Chem. Phys.* **2009**, *130*, 114903.
(42) Zhang, C.; Chu, X.; Zheng, Z.; Jia, P.; Zhao, J. Diffusion of Ionic Fluorescent Probes atop Polyelectrolyte Brushes. *J. Phys. Chem. B* **2011**, *115*, 15167−15173.
(43) Wang, S.; Jing, B.; Zhu, Y. Molecule Motion at Polymer Brush Interfaces from Single-Molecule Experimental Perspectives. *J. Polym. Sci., Part B: Polym. Phys.* **2014**, *52*, 85−103.
(44) Carr, J. K.; Himes, R. D.; Keung, C. H.; Burden, D. L.; Walhout, P. K. Heterogeneous Translational Dynamics of Rhodamine B in Polyelectrolyte Multilayer Thin Films Observed by Single Molecule Microscopy. *Langmuir* **2009**, *25*, 8330−8339.
(45) Ghostine, R. A.; Schlenoff, J. B. Ion Diffusion Coefficients Through Polyelectrolyte Multilayers: Temperature and Charge Dependence. *Langmuir* **2011**, *27*, 8241−8247.
(46) Kisley, L.; Chang, W.-S.; Cooper, D.; Mansur, A. P.; Landes, C. F. Extending Single Molecule Fluorescence Observation Time by Amplitude-Modulated Excitation. *Methods Appl. Fluoresc.* **2013**, *1*, 037001.
(47) Shuang, B.; Chen, J.; Kisley, L.; Landes, C. F. Troika of Single Particle Tracking Programing: SNR Enhancement, Particle Identification, and Mapping. *Phys. Chem. Chem. Phys.* **2014**, *16*, 624−634.
(48) Chen, J.; Bremauntz, A.; Kisley, L.; Shuang, B.; Landes, C. F. Super-Resolution mbPAINT for Optical Localization of Single-Stranded DNA. *ACS Appl. Mater. Interfaces* **2013**, *5*, 9338−9343.
(49) Kisley, L.; Chen, J.; Mansur, A. P.; Shuang, B.; Kourentzi, K.; Poongavanam, M.-V.; Chen, W.-H.; Dhamane, S.; Willson, R. C.; Landes, C. F. Unified Superresolution Experiments and Stochastic Theory Provide Mechanistic Insight into Protein Ion-Exchange Adsorptive Separations. *Proc. Natl. Acad. Sci. U. S. A.* **2014**, *111*, 2075−2080.
(50) Chenouard, N.; Smal, I.; de Chaumont, F.; Maska, M.; Sbalzarini, I. F.; Gong, Y.; Cardinale, J.; Carthel, C.; Coraluppi, S.; Winter, M.; et al. Objective Comparison of Particle Tracking Methods. *Nat. Methods* **2014**, *11*, 281−289.
(51) Parthasarathy, R. Rapid, Accurate Particle Tracking by Calculation of Radial Symmetry Centers. *Nat. Methods* **2012**, *9*, 724−726.
(52) Crocker, J. C.; Grier, D. G. Methods of Digital Video Microscopy for Colloidal Studies. *J. Colloid Interface Sci.* **1996**, *179*, 298−310.
(53) Burke, S. E.; Barrett, C. J. Acid−Base Equilibria of Weak Polyelectrolytes in Multilayer Thin Films. *Langmuir* **2003**, *19*, 3297−3303.
(54) Ghostine, R. A.; Markarian, M. Z.; Schlenoff, J. B. Asymmetric Growth in Polyelectrolyte Multilayers. *J. Am. Chem. Soc.* **2013**, *135*, 7636−7646.
(55) Khurana, T. K.; Santiago, J. G. Effects of Carbon Dioxide on Peak Mode Isotachophoresis: Simultaneous Preconcentration and Separation. *Lab Chip* **2009**, *9*, 1377−1384.
(56) Cooper, J. T.; Peterson, E. M.; Harris, J. M. Fluorescence Imaging of Single-Molecule Retention Trajectories in Reversed Phase Chromatographic Particles. *Anal. Chem.* **2013**, *85*, 9363−9370.
(57) Elliott, L. C. C.; Barhoum, M.; Harris, J. M.; Bohn, P. W. Trajectory Analysis of Single Molecules Exhibiting Non-Brownian Motion. *Phys. Chem. Chem. Phys.* **2011**, *13*, 4326−4334.
(58) Shuang, B.; Byers, C. P.; Kisley, L.; Wang, L.-Y.; Zhao, J.; Morimura, H.; Link, S.; Landes, C. F. Improved Analysis for Determining Diffusion Coefficients from Short, Single-Molecule Trajectories with Photoblinking. *Langmuir* **2012**, *29*, 228−234.
(59) Li, Y.; Yip, W. T. Coulombic Interactions on the Deposition and Rotational Mobility Distributions of Dyes in Polyelectrolyte Multilayer Thin Films. *Langmuir* **2004**, *20*, 11039−11045.
(60) Sukhishvili, S. A. Responsive Polymer Films and Capsules via Layer-by-Layer Assembly. *Curr. Opin. Colloid Interface Sci.* **2005**, *10*, 37−44.